



Heriot-Watt University  
Research Gateway

# Assessment of compliance of dimensional tolerances in concrete slabs using TLS data and the 2D continuous wavelet transform

**Citation for published version:**

Puri, N, Valero, E, Turkan, Y & Bosché, FN 2018, 'Assessment of compliance of dimensional tolerances in concrete slabs using TLS data and the 2D continuous wavelet transform', *Automation in Construction*, vol. 94, pp. 62-72. <https://doi.org/10.1016/j.autcon.2018.06.004>

**Digital Object Identifier (DOI):**

[10.1016/j.autcon.2018.06.004](https://doi.org/10.1016/j.autcon.2018.06.004)

**Link:**

[Link to publication record in Heriot-Watt Research Portal](#)

**Document Version:**

Peer reviewed version

**Published In:**

Automation in Construction

**Publisher Rights Statement:**

© 2018 Elsevier B.V.

**General rights**

Copyright for the publications made accessible via Heriot-Watt Research Portal is retained by the author(s) and / or other copyright owners and it is a condition of accessing these publications that users recognise and abide by the legal requirements associated with these rights.

**Take down policy**

Heriot-Watt University has made every reasonable effort to ensure that the content in Heriot-Watt Research Portal complies with UK legislation. If you believe that the public display of this file breaches copyright please contact [open.access@hw.ac.uk](mailto:open.access@hw.ac.uk) providing details, and we will remove access to the work immediately and investigate your claim.

## **Assessment of Compliance of Dimensional Tolerances in Concrete Slabs using TLS data and the 2D Continuous Wavelet Transform**

Nisha Puri<sup>a</sup>, Enrique Valero<sup>b</sup>, Yelda Turkan<sup>a\*</sup>, Frédéric Bosché<sup>b</sup>

<sup>a</sup> *School of Civil and Construction Engineering, Oregon State University, Corvallis, OR 97331, USA*

<sup>b</sup> *School of Energy, Geoscience, Infrastructure and Society, Heriot-Watt University, Edinburgh EH14 4AS, UK*

### **Abstract**

While several concrete waviness assessment methods are being developed to overcome the disadvantages of one assessment method over the other, the sparseness of measurements associated with each method prevents from achieving a better understanding of how elevations and undulations change across the surface. Assessing waviness over multiple one-dimensional (1D)-survey lines may not accurately reflect the actual condition or waviness of the entire floor. The methodology presented in this paper presents a compliance-checking algorithm for detecting elements where dimensions exceed specified tolerance. It also enables assessment of a concrete surface in two-dimensional (2D) domain using the synergy of Terrestrial Laser Scanning (TLS) and Continuous Wavelet Transform (CWT). 2D CWT analysis provides information not only about the periods of the surface undulation, but also the location of such undulations. The validity of the methodology is established by running a test on point clouds obtained from a warehouse project near Gresham, Oregon. A rigorous comparison between one of the existing floor waviness measurement methods, the waviness index method, and the proposed method is made. The results showed that the proposed methodology delivers accurate results that enable the localization of surface undulations of various characteristic periods. Furthermore, the proposed method is more efficient in terms of time taken for acquiring the measurements, and is, thus, more cost efficient.

**Keywords:** Dimensional Quality Control, Tolerance Compliance, Terrestrial Laser Scanning, Point Cloud, Continuous Wavelet Transform, Depth Map

---

\* Corresponding author. Tel: +1 541 737 2631; E-mail addresses: [purin@oregonstate.edu](mailto:purin@oregonstate.edu) (N. Puri); [E.Valero@hw.ac.uk](mailto:E.Valero@hw.ac.uk) (E. Valero); [yelda.turkan@oregonstate.edu](mailto:yelda.turkan@oregonstate.edu) (Y. Turkan); [F.N.Bosche@hw.ac.uk](mailto:F.N.Bosche@hw.ac.uk) (F. Bosche).

# 1 Introduction

As-built dimensions of cast-in-place concrete elements often differ from the dimensions originally specified in as-designed plans [1]. Dimensional Quality Control (QC) verifies that elements are constructed in compliance with the specified dimensional tolerances. For instance, when combining precast and cast-in-place elements, checking dimensional tolerance of all elements is necessary for ensuring acceptable performance of joints and interfacing materials [2]. In addition, failure to detect the imperfections in newly constructed surfaces during the earlier stages of construction causes delays in carrying out necessary repair works [3]. The repair, demolition, removal and replacement of defective concrete elements entail additional costs that could amount to as much as 12% of the project contract value [3-6]. Thus, upon the completion of concrete elements, it is crucial to carry out inspections in a timely manner. Furthermore, traditional inspection procedures related to dimensional QC are labor intensive and time consuming.

Focusing on concrete slabs, several factors influence the dimensional quality of cast-in-place concrete slabs, such as sweltering temperatures, placement and finishing techniques that are applied during construction. Proper regulation and control of these factors are essential for achieving specified levels of waviness and levelness. The defects resulting from the waviness of concrete slabs not only create aesthetic issues but also affect the efficiency of lift trucks and very narrow aisle (VNA) vehicles. Even if waviness present in slabs is not immediately noticeable, the waviness of the concrete slabs in industrial facilities, such as large warehouses, must be strictly examined since failing to detect waviness and deviations from the specified tolerances can greatly affect the operational activities that the floor is designed to handle [8]. Figure 1 illustrates how irregularities on the floor affect the stability of VNA trucks. Variations in elevation between the left and right wheels ( $d$ ) of a VNA truck results in static lean ( $s$ ) of VNA trucks. The static lean can potentially increase up to ten times due to the waviness present in concrete slabs [9].

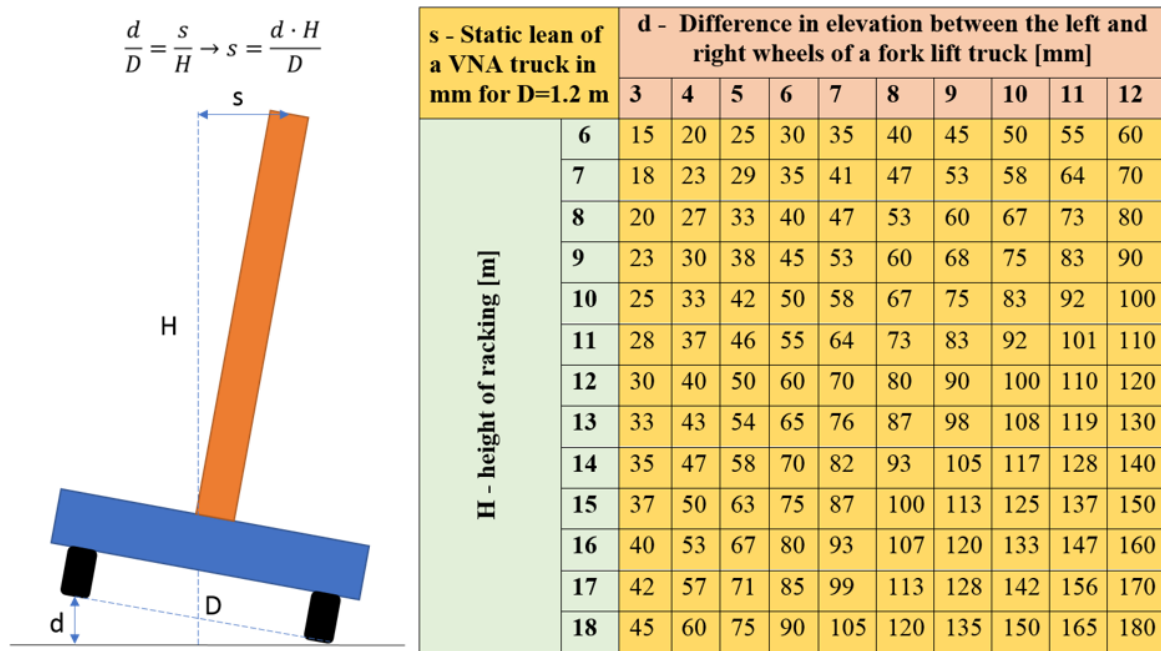


Figure 1 The effect of difference in elevation between the wheels on the static lean for a VNA

The methods for measuring concrete slab waviness, which are currently prevalent in the construction industry, require intensive human intervention, are tedious and time-consuming, and yet are based on sparse measurements. These methods entail the surveying of 1D lines for differences in elevations and characterizing undulations of specific periods.

The Straightedge method involves laying a 10-ft (3.05 m) Straightedge across a survey line on the floor and measuring the distance between the Straightedge and the floor using a stainless steel slip gauge [1]. While the results obtained with this method are easily comprehensible, the process of laying out the Straightedge over large surface areas is labor-intensive and engenders random errors in the measurements [10]. In addition, this time-intensive method provides information about the deviations between as-built and as-designed points only at relatively few measured points.

The introduction of the F-numbers method was aimed towards eradicating random errors in measurements, via the use of instruments that enable measurement of elevation differences at fix intervals to produce more accurate results. It provides the results in the form of two numbers: Floor Flatness (FF) and Floor Levelness (FL). FF describes the flatness associated with the measured floor surface point, whereas FL describes the levelness of the measured floor surface point. As

described in the ASTM E1155-14 standard [11], the measurements are carried out at intervals of 1-ft along each survey line, and the measurements collected from multiple survey lines are statistically processed to generate FF and FL numbers that describe the conditions of the entire floor surface. In addition, results produced from the F-number method are in the form of flatness numbers ( $F_F$  and  $F_L$  values) that are hard to comprehend.

The Waviness Index (WI) method, as described in ASTM E1486-14 [12], was developed later because the F-number method provides information only about the floor undulations with periods of 1.5 to 4-ft (0.46 – 1.22 m) and 15 to 80-ft (4.6 – 24.4 m). In contrast, the WI method identifies various periods of floor undulations between 2-ft and 10-ft, which correspond to the periods of surface undulation that affect the operation of forklifts [13][8][14]. The results obtained using the WI method are expressed in inches and are relatively easier to comprehend.

Despite having a significant advantage over the Straightedge and the F-number methods, the WI method shares similar drawbacks with those methods. Sparse measurements yielded by the three methods fail to guarantee that the collected data is an accurate representation of the geometric features of the surface. Although results may be repeatable with a certain error, they fail to capture the geometric details of the entire 2D floor surface and essentially do not impart information about the waviness of the 2D surface. Data collection from large surface areas using these methods demands significant amount of time and manual labor. Since these methods require measurement tools to be manually moved across the surface of the floor, the results obtained are prone to human error. Random errors, which potentially arise due to possible carelessness exerted while handling the measurement instruments, contribute toward inaccuracies in measurements. Moreover, the inability to retrieve similar results between different measurement sessions is one of the prominent drawbacks of these methods. And finally, applying these methods to measure the floor waviness of large floor areas, such as warehouse projects, is quite difficult. It is important to note that warehouse projects typically have floor surface areas that are larger than 4,000 m<sup>2</sup>. Consequently, using these methods for such projects generate results that are not repeatable. In addition, the obtained results are limited in the orientation of the defects and the range of wavelength. Furthermore, the inability to explicitly reveal the location of those undulations remains a disadvantage for these methods [8].

The F-number and WI methods reflect the state-of-the-art practices in measuring the waviness of concrete slabs. To overcome the challenges arising with these methods, newer technologies, such as terrestrial laser scanning (TLS), can be leveraged to measure surface waviness in a more efficient manner. The ability of a TLS device to accurately capture the geometric information of concrete surfaces provides an opportunity to reconsider the assessment of surface waviness using traditional measurement instruments.

The objective of this study is to develop a methodology that uses TLS to obtain accurate waviness information about newly constructed and existing concrete surfaces rapidly. This paper presents a methodology that applies the two-dimensional Continuous Wavelet Transform (2D CWT) to TLS point clouds to measure concrete slab surface waviness. The proposed methodology is designed to help carry out tolerance compliance control tasks for slabs based on project specifications describing their waviness tolerances. Uniquely, the methodology is able to perform an accurate and comprehensive assessment of the surface geometry in both spatial and frequency domains. The features pertaining to the proposed and existing methods are summarized in Table 1.

Table 1 Features and performance of existing standard methods and the proposed method for measuring floor flatness.

	Method	Straightedge	F-Number	Waviness Index	2D CWT
<b>Features</b>	<b>Periods of undulation detected</b>	10'-20' (3.05 – 6.10 m)	1.5' – 4' (0.46 – 1.22 m) ( $F_F$ ) 15' – 80' (4.57 – 24.38 m). ( $F_L$ )	2' – 10' (0.61 – 3.05 m)	Any
	<b>Output</b>	Values in Inches	$F_F$ and $F_L$ values	Values in Inches	Map showing detected undulations for various periods
	<b>Types of errors</b>	Random and systematic error	Random error	Random error	Systematic error ( $\pm 3$ to $\pm 6$ mm)

<b>Performance Criteria Achievement</b>	<b>Data acquisition efficiency (approx.) (sec/m<sup>2</sup>)</b>	7	4	4	2
	<b>Point Sampling</b>	Along 1D non-parallel survey lines in 10-foot segments	Along 1D parallel survey lines in two orthogonal directions	Along 1D parallel survey lines in two orthogonal directions	Across 2D surface
	<b>Sparsity of measurements</b>	No	No	No	Yes
	<b>Localization of defects</b>	No	No	No	Yes
	<b>Visualization of region of defects</b>	No	No	No	Yes
	<b>Repeatability</b>	No	No	No	Yes

89

90           The rest of the paper is structured as follows. Section 2 provides background information  
91 on the utilization of TLS point clouds for project and QC, and the application of discrete and  
92 continuous wavelet transforms for surface characterization. Section 3 then introduces the proposed  
93 method for characterizing surface waviness of concrete slabs and discusses the various stages of  
94 pre-processing and processing the TLS point cloud data. The proposed methodology is validated  
95 using data obtained from a warehouse construction project. The experimental results are provided  
96 and discussed in Section 4. The final section draws conclusions and discusses directions for future  
97 research.

## 98    **2   Research Background**

### 99    **2.1   Dimensional Tolerances for Floor Flatness and Waviness**

100            The dimensions of newly constructed and existing building elements can vary, slightly or  
101 significantly, from the dimensions specified in the design documents [1]. Tolerances, or allowable  
102 deviations in those dimensions, are typically specified during the design phase for different  
103 measures such as length, width, thickness, perpendicularity, or verticality. Standard ACI 117-90,  
104 for example, provides a comprehensive list of tolerance criteria for cast-in-place concrete  
105 elements, such as vertical, lateral, and level alignments, and cross-sectional dimensions. The  
106 specified dimensional tolerances are an output of economical and practical considerations [15].  
107 The role of QC inspectors is to ensure that the appropriate/specified tolerance values are achieved  
108 as construction progresses. Inaccuracies in the geometry of concrete elements during construction  
109 arise from improper establishment of a reference system for controlling the alignment, manual  
110 measurements, poor workmanship and in some cases, the method used for measurement [16].

### 111    **2.2   TLS Point Clouds for Project Control**

112            Acquisition of accurate project as-built data is crucial for dimensional quality control  
113 measurements, so that informed decisions can be made in a timely manner. TLS is a modern  
114 surveying technology that has been gaining increasing popularity in the Architectural,  
115 Engineering, Construction and Facilities Management (AEC&FM) industry. The versatility of the  
116 TLS technology has been tested in various fields of AEC&FM. For example, TLS has been used  
117 in remotely assessing the conditions of environments where human access is difficult or dangerous  
118 [17], for generating BIMs that represent the as-built conditions of building facilities [18], as well  
119 as construction progress control [15–19].

#### 120    **2.2.1   TLS Point Clouds for Quality Control**

121            The use of TLS for dimensional QC is gaining interest due to its ability to rapidly provide  
122 inspectors with project as-built data in the form of both dense and accurate 3D point clouds (sub  
123 mm to mm-level accuracy) [24]. Using TLS not only solves the problems associated with accuracy  
124 and repeatability, but also enables the acquisition of data that represents the geometry of entire  
125 surfaces, thereby addressing the data sparsity limitations of existing surveying methods. Focusing



on flatness measurement, compared to existing measurement tools employed in current standard flatness measurement methods, TLS thus offers an efficient way of collecting dense as-built data covering entire slab surface.

Regarding the processing of TLS data for QC, Fuchs et al. [25] and Shafer and Weber [26] developed deformation monitoring algorithms to find the differences in positions of TLS data points with respect to a reference surface. In [27], a color map generated from the TLS data was used to assess the flatness of facades in a multi-story building and the additional costs arising from placing excess mortar on these facades was evaluated based on the volumetric quantities derived from TLS data. In [28], a methodology that identifies the geometric irregularities in precast concrete elements by comparing as-built data obtained from TLS and as-designed data obtained from BIM was developed. Tang et al. [7] developed three algorithms which helped in finding the difference in elevation of the points in the point cloud with respect to a plane taken from a BIM model or a plane specified by the user. The method described in [29] used an elevation map where each interval in height were represented with different colors. This approach represented the height of each point with respect to a reference plane obtained from a BIM model. All the proposed methodologies and existing approaches detected areas where different degrees of deviations occurred, however they have failed to characterize the waviness or the periods of surface undulations.

Using 3D point clouds obtained from TLS and as-designed geometry information from BIM, Bosché and Guenet [30] developed an approach based on BIM and TLS data to assess whether the geometry of as-is elements adhere to the specified surface flatness tolerances. An experiment was conducted to compare the results obtained using the proposed method with the ones obtained from Straightedge and F-number methods. [The digital application of Straightedge and F-Number, as presented in that study, significantly reduces the time required for data collection and analysis, compared to traditional methods. However, flatness analysis remains conducted along sparsely surveyed 1D survey lines, which delivers results limited in spatial and wavelength resolution.](#) Bosché and Biotteau [8] developed a method that applies 1D CWT to TLS data to characterize surface undulation periods. [That approach addresses the limitation of previous works in wavelength resolution, i.e. the approach examines surface waviness at a wider range of wavelengths or characteristic periods. However, the study remains based on measurements along](#)

1D lines that do not enable an analysis of flatness in all possible directions, and still provide results with limited spatial resolution. Valero and Bosche [31] presented preliminary results on the application of the 2D CWT to TLS data and compared the results with the WI method using laboratory experiments. The work presented here expands on this and delivers a 2D analysis of surface data in a more comprehensive manner using a larger and more representative concrete slab as case study.

### 2.3 Wavelet Transform for Surface Characterization

Wavelet Transform (WT) has a wide range of applications in engineering, some of which include seismic signal analysis [32], sound pattern analysis [33] and quantum mechanics [34]. WT is also widely used in the area of surface texture characterization, where it is used to break down the 2D profiles of surfaces into the roughness and waviness components [35]. WT has been applied to characterize surface roughness and waviness in several studies, and it has many applications in the field of point cloud processing such as point cloud de-noising and rock surface roughness quantification [31–33]. A technique using 1D WT for characterizing different types of surfaces was introduced by Chen et al. [39]. Josso et al. [40] performed 2D multi-scaled decomposition using images instead of profiles. Stepień and Makiela [41] applied 2D WT to analyze the deviations of cylindrical surfaces. Jiang et al. [42], Coiffman and Maggioni [43] and Hussein et al. [44] described the concepts of lifting wavelets and diffusion wavelets and used them for surface filtering. WT can be extended from 1D analysis to multi-dimensional signals as well [8][45]. Some applications of 2D CWT include characterizing the wavelengths of landslide areas and identifying the regions having high risk of landslides using topographic images [46]. Additional information about the different types of wavelets and the application of wavelet transform, can be found in [47] and [48]. And, as reviewed above, the CWT has been previously suggested in [8] and [31] for use in construction surface flatness assessment.

### 2.4 Continuous Wavelet Transform

The continuous wavelet transform (CWT) of a given function is the inner product of the function with the scaled and shifted versions of the mother wavelet [47]. The output of the inner product is the wavelet coefficient at a specific time or location and scale [48]. In order for a

function,  $\psi(t) \in L^2(\mathbb{R})$ , to qualify as a mother wavelet, it has to satisfy a condition known as the admissibility condition as stated below [49]:

$$0 < C_\psi = \int_{-\infty}^{\infty} \frac{|\psi(\omega)|}{|\omega|} d\omega < \infty \quad (1)$$

where,  $C_\psi$  is the admissibility condition and  $\omega$  is the angular (or radian) frequency. This condition can also be written as [49]:

$$\Psi(0) = \int_{-\infty}^{\infty} \psi(t) dt = 0 \quad (2)$$

This implies that the function  $\psi(t)$  has to move above and below the  $t$ -axis in a wave-like manner with decaying properties. Figure 2 demonstrates such properties with the example of a typical wavelet function commonly known as the Mexican Hat wavelet.

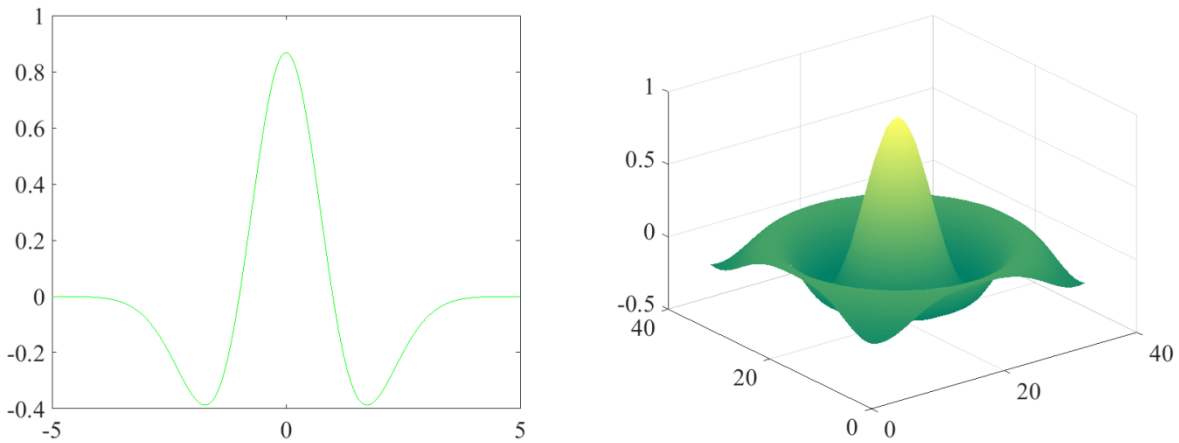


Figure 2 1D (left) and 2D (right) Mexican Hat Wavelet

CWT can be used to describe the time and frequency components of a temporal signal in detail. 1D CWT involves taking the original function and displaying the output function in terms of two variables, which are time and scale. The spectral information about a 2D signal for any scale  $s$  and location  $(x, y)$  is given by the 2D CWT [50], that is an extension of the 1D CWT and can be represented as follows [51]:

$$CWT(a, b, s) = \frac{1}{s} \int_{-\infty}^{\infty} \int_{-\infty}^{\infty} g(x, y) \psi_{abs}(x, y) dx dy \quad (3)$$

where,  $\psi_{abs}(x, y)$  is the mother wavelet,  $g(x, y)$  is the continuous 2D signal,  $s$  is the scale (dilating parameter) and  $(a, b)$  represents the location (translating parameter).

Different values of the translating and dilating parameters of the mother wavelet help in describing the different frequencies of undulations present in the surface [52]. The convolution of  $\psi$  and  $g$  provides the wavelengths (or periods) of the undulations present in the surface. The coefficients  $CWT(a, b, s)$  quantify the degree of correlation between the wavelet  $\psi$  and the function  $g$  at each point. In this way, apart from analyzing signals in time and frequency, the CWT can be extended to analyze signals, together in space and scale (space-scale analysis).

Different wavelets can be used as the mother wavelet to detect different types of undulations. The selection of an appropriate type of wavelet determines how efficiently the different components of a signal are extracted [53]. The geometric shapes of the wavelet is considered an important criteria when selecting the type of mother wavelet in [54]. The resemblance between the shape of the wavelet and the geometric features of a signal provides a cue for the selection of an appropriate wavelet. The defects present in as-built or as-is concrete surfaces resembles waves in the form of small bumps and dips, and the shape of 2D Mexican Hat wavelet closely resembles the shape of the surface undulations present on concrete surfaces, as shown in Figure 2. The Mexican Hat wavelet is a real and isotropic wavelet that is good for detecting contour features [55][56]. The use of different values of the translation and scale parameters of the mother wavelet enable the detection of undulations corresponding to different characteristic periods in the point cloud data. Therefore, it is chosen as the mother wavelet in this study. 2D Mexican Hat wavelet in spatial domain is depicted as follows:

$$\psi(x,y) = \frac{1}{2\pi}(2 - x^2 - y^2) * e^{-\frac{1}{2}(x^2 + y^2)} \quad (4)$$

## 2.5 Contribution

Floor flatness testing is typically performed to assess how well the contractor has performed the work based on the specifications. Failure to carry out floor flatness measurements within a specific time window may yield inaccurate results and does not accurately reflect the contractor's performance. This can be attributed to the increase in curling of the joints and cracks in the concrete slabs with the age of concrete. Therefore, the American Concrete Institute (ACI 117-10) [57] requires that floor flatness testing on any concrete slab should be performed within 24 hours for

best results, and no later than 72 hours, after the concrete placement, unless clearly stated otherwise in the specifications.

The major contribution of this paper is to present a new approach for floor flatness control using the 2D CWT applied to TLS data. The approach builds on preliminary works published in [33], but presents and analyses it in a more comprehensive manner. In particular, a warehouse concrete slab having been scanned within 10 hours of having been poured is used as a representative real-life case study. The overall time required for scanning the worksite is less than the time associated with data collection using the traditional methods of waviness measurement. The waviness results obtained using the proposed approach are validated by establishing a correlation between results obtained using the proposed approach and the WI method. The correlation shows that the proposed method generates results that supersede those that are obtained using the WI method.

### **3 Proposed Methodology**

The proposed methodology, as summarized in Figure 3, follows the approaches developed in [31] in order to characterize surface waviness. The raw 3D point cloud consists of data points from a concrete slab as well as its surrounding environment, including workers, equipment and surrounding buildings. The point cloud is typically the result of multiple laser scans co-registered using a standard (reliable) target-based approach. First, the raw point cloud is pre-processed to isolate the area of interest, the concrete slab in this case, from the raw point cloud. The next step is to develop a depth map, which is used as input to the 2D CWT. The areas with undulations corresponding to various characteristic periods are identified after applying the 2D CWT with the Mexican Hat wavelet.

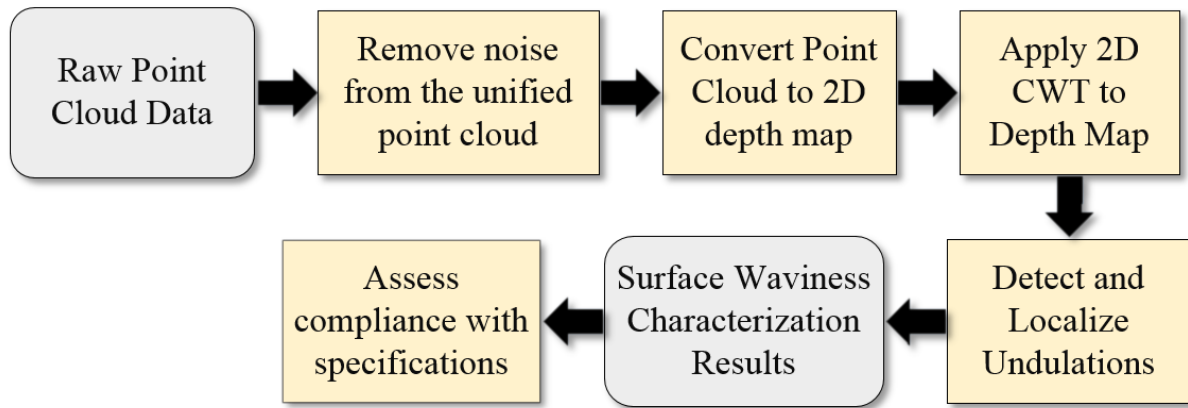


Figure 3 Overview of the research methodology

### 3.1 Data pre-processing

As stated in the overview of the research methodology, the raw point cloud data should be pre-processed before 2D CWT can be applied to it. The input is a raw point cloud that may be the result of the co-registration of multiple scans collected during the scanning process. The noise present in the registered point cloud data is removed using a corresponding functionality provided by a commercial point cloud processing software, leaving a clean point cloud of the area of interest (i.e. concrete slab). The pre-processed point cloud corresponding to the slab surface is aligned (parallel) to the  $xy$  plane, which is likely to be the case already. Accordingly,  $z$  coordinates represent the elevation of each point, facilitating further analysis.

In order to analyze the frequencies of undulations present on the surface, the point cloud data should have equispaced rows and columns along the  $x$  and  $y$  axes [58]. Because raw point cloud data from slabs typically has a random arrangement, it is converted into a regular grid, with intervals along the  $x$  and  $y$  axes were both set to  $\delta_p = 1$  cm. This sampling interval ensures robust localization of defects across the 2D surface. Triangulation-based linear interpolation is used to obtain the values of  $z$ -coordinates at each grid point. Consequently, a 2D depth map is created, which represents the height of the surface for points at  $\delta_p = 1$  cm intervals along the  $x$ - and  $y$ -axes.

## 3.2 Detection of Undulations using 2D Continuous Wavelet Transform

The depth map resulting from the previous operation is used as the input “signal” to the 2D CWT. The scale  $a$  at which the CWT is applied relates to a few parameters, as in Equation 5 [48]:

$$a = \frac{f_c}{f \cdot \delta_p} = \frac{T \cdot f_c}{\delta_p} \quad (5)$$

where  $f$  represents the frequency of the undulation,  $T$  the characteristic period of the signal, and  $f_c$ , the main frequency component of the Fourier Transform of the mother wavelet. For the Mexican Hat wavelet,  $f_c = 0.252 \text{ cm}^{-1}$ .

The output of applying the 2D CWT is a series of scalograms that report the CWT response at each grid point on the depth map. These maps are meaningful to some extent, but should be further processed to accurately define the exact characteristic period at each location. Indeed, a wavy region will result in peak responses at several scales, i.e. frequencies, as can be seen in Figure 77 for example. However, not all those peaks correspond to defects whose size matches the period associated to that scale. For this, we follow the strategy initially suggested in Valero and Bosché in [31]. First, peak values (i.e. local maxima) are detected in each 2D CWT response map. Next, different isolines are then calculated around each peak, which connect pixels with the same CWT response. These isolines may describe irregular shapes whose mathematical analysis, and further comparison with other defects, can be truly complex. Therefore, areas enclosed by isolines are described by means of ellipses, and the two main axes of each ellipse are determined to be used as reference values. If any of the axes matches the period associated to the scale of interest, a surface deviation is detected in that area for that particular period.

The result of this process is a set of clear waviness defect detections at all the scales/periods considered, which can be combined in a single diagram.

## 3.3 Correspondence between WI and 2D CWT methods.

The correspondence between the WI method and the 2D CWT method in terms of their response to similar surface wavelengths (or periods) is shown in Table 2. The  $k$  values of the WI method correspond to characteristic periods of different lengths. The corresponding CWT scales for each of these  $k$  values are calculated using equation 5 with  $\delta_p = 1 \text{ cm}$ . The characteristic

periods ( $T$ ) selected in this table represent the floor undulations, with periods of 2, 4, 6, 8 and 10 ft, that are the focus of the WI method.

Table 2 Continuous Wavelet Transform scales and equivalent Waviness Index [8]

Characteristic period ( $T$ ) [cm]	CWT scale ( $a$ )	Waviness Index ( $k$ values)
61	15	1
121.9	30	2
182.9	45	3
243.8	60	4
304.8	75	5

## 4 Experimental Results

### 4.1 Data Collection and Pre-Processing

An in-situ concrete slab from a warehouse project in Gresham, Oregon was scanned after 5-6 hours of placement. The surface of the concrete slab was sturdy enough for foot traffic and for setting up the tripod of the scanner. The concrete slab of the warehouse building was scanned using a Leica ScanStation P40 3D laser scanner. The scanner has 8" horizontal and 8" vertical angular accuracy. The 3D position accuracy is  $\pm 3$ mm at 50 m and  $\pm 6$  mm at 100 m [59].

Figure 4 shows the plan view of the concrete slab as well as one of the 3D point clouds captured. The area of interest with a surface area of approximately 1500 m<sup>2</sup> is highlighted in both the plan view and the point cloud. It was determined that scans taken from four different locations would be sufficient to capture the surface with sufficient detail. Six targets were placed at different locations on site to facilitate the point cloud registration process.



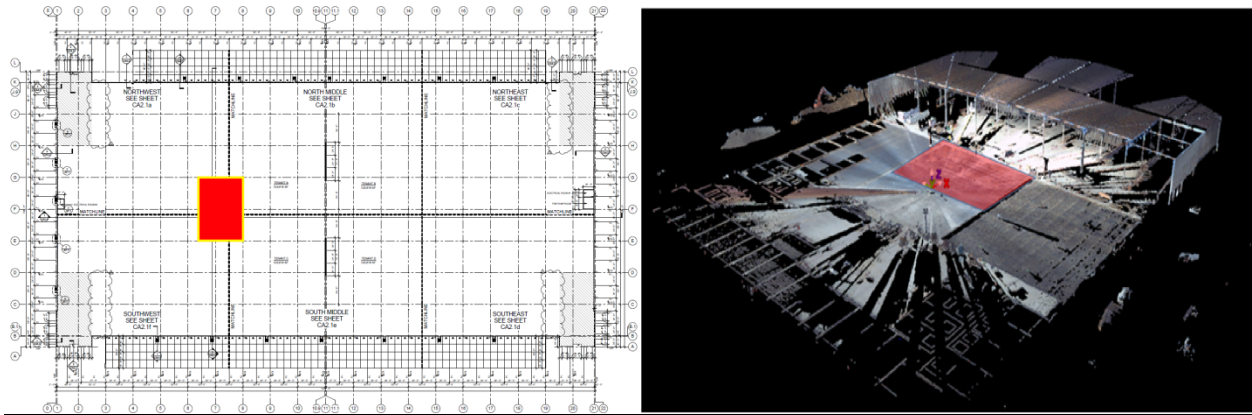


Figure 4 The floor plan (left) and the 3D point cloud (right) of the warehouse building. The area of interest is highlighted in red.

The overall scanning process, including setup, scanning, dismantling and re-locating, took approximately 45 minutes. The data pre-processing stage, comprising of registering the point clouds in the same coordinate system and removing the noise, took 50 minutes. The raw point clouds, i.e. laser scans including noise, were first imported into a commercial point cloud processing software. The four laser scans were registered under the same coordinate system using the targets placed at strategic locations on the construction site. After the registration was complete, the point cloud of the area of interest was manually isolated from the rest. The point cloud corresponding to the slab section of interest had approximately 100,000,000 points. Figure 5 shows an image of the scan after registration and noise removal.

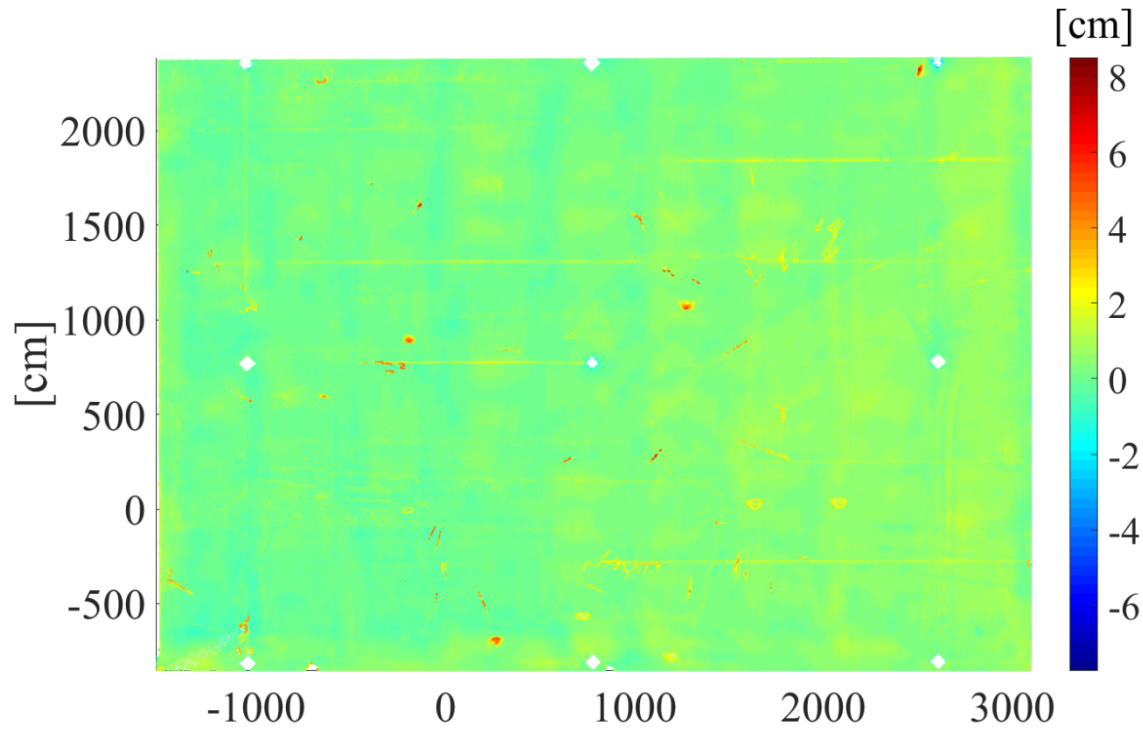


Figure 5 Top view of the point cloud of the area of interest obtained after the registration of the four scans and noise removal. The color scale represents elevation values in cm.

## 4.2 Data Processing

Following pre-processing, the point cloud is converted into a 3242 x 4629 depth map with 1 cm intervals in both horizontal and vertical directions, with the  $z$ -coordinates at each grid point calculated as described in Section 3.1. Figure 6 shows the resulting depth map. As seen in Figure 6, the height of the concrete slab with respect to the  $xy$  plane, varies most in the interval of -2 cm to 2 cm. Thus, the color map was adjusted accordingly to highlight the height differences between various areas across the floor.

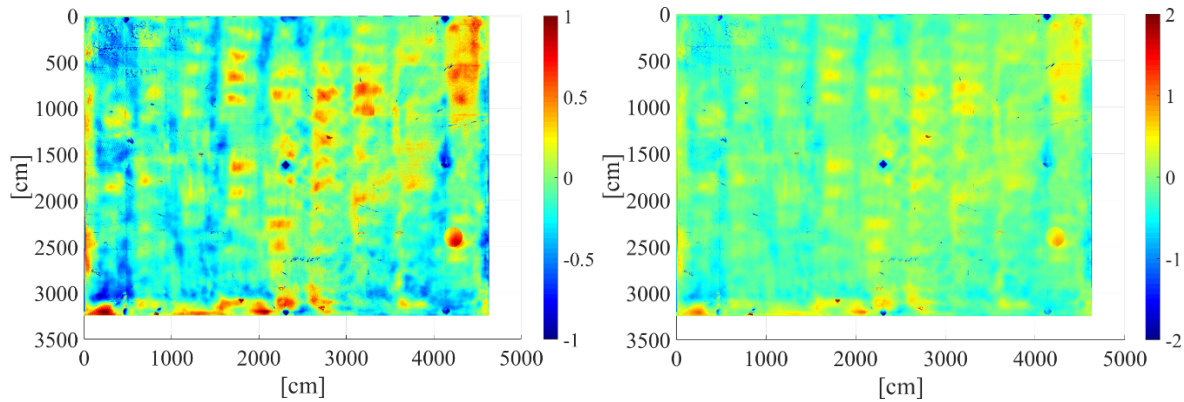


Figure 6 Depth map derived from the TLS data, with color map limits set to  $[-1, 1]$  cm (left) and  $[-2, 2]$  cm (right)

### 4.3 CWT Results

#### 4.3.1 CWT Scalogram

Figure 7 presents the results obtained using the scales (a) 15, 30, 45, 60 and 75 of the mother wavelet. The regions where the input “signal” strongly correlates with the mother wavelet applied at the scales above are highlighted in yellow in Figure 7.

The point cloud in Figure 5 and the depth maps in Figure 6 show that the surface of the investigated slab is relatively flat with a few “peaks”. For the entire slab surface, the average value of the deviation in the z-axis was 0.0 cm with a standard deviation of 0.3 cm. Figure 7(a) represents the regions where the wavelength of the undulations present on the surface correlates with the mother wavelet of scale 15. The scalogram shows that the regions near (1900 cm, 3100 cm) has an undulation of this characteristic period present on the slab surface. Figure 7 (b) shows regions near (1900 cm, 3100 cm) and (2400 cm, 1700 cm) have undulations that correspond to the mother wavelet of scale 30. Similarly, the scalograms in Figure 7 (c), (d) and (e) show that the region near (2400 cm, 1700 cm), (300 cm, 3400 cm) and (4200 cm, 2400 cm) have undulations corresponding to scales 45, 60 and 75. The region near (2400 cm, 1700 cm) shows responses for all these three scales. Thus, the identification of the scale which has the top response at that location is necessary. Furthermore, such analysis is an added advantage of using the proposed 2D CWT method and cannot be done using the WI method.

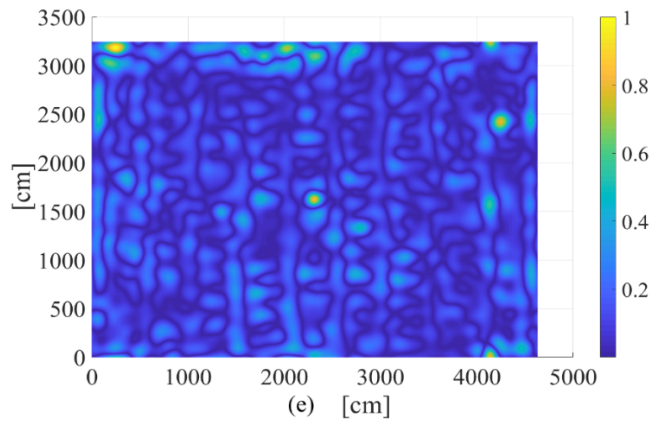
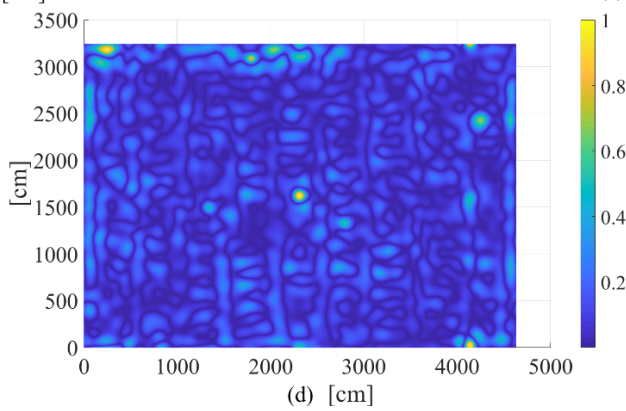
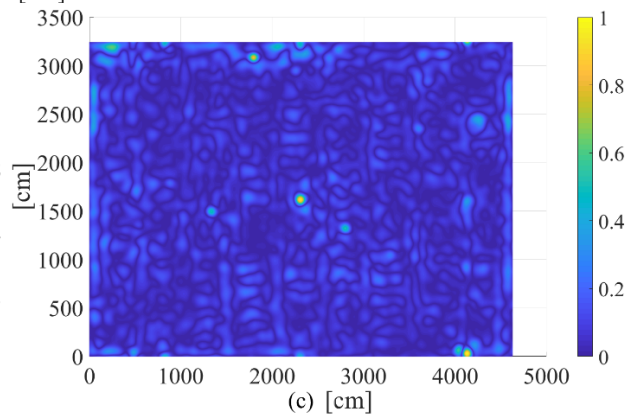
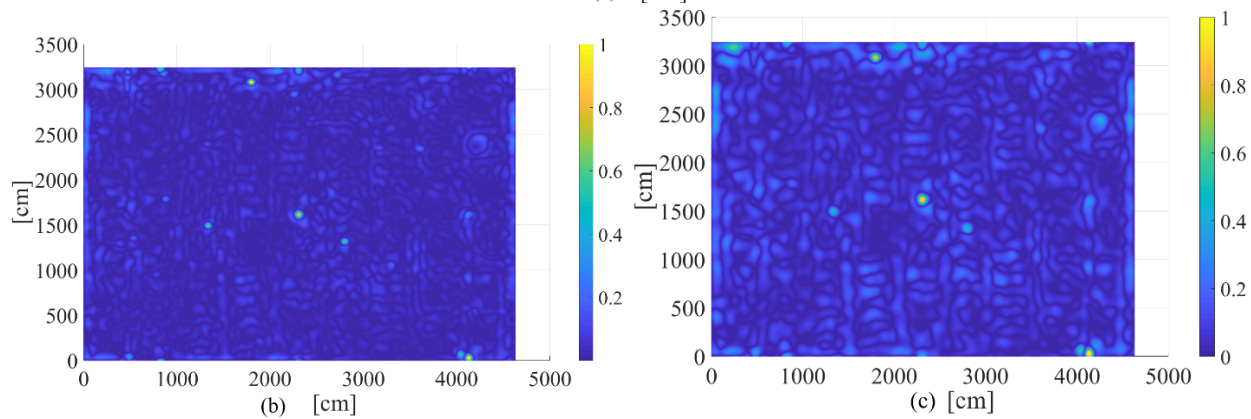
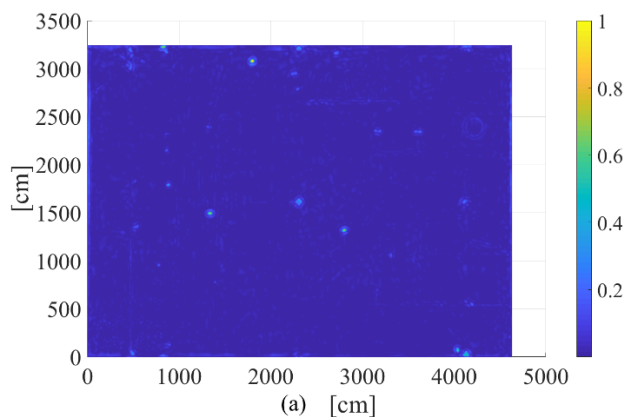


Figure 7 The coefficients obtained from the wavelet transformation corresponding to scales 15 (a), 30 (b), 45 (c), 60 (d) and 75 (e) are plotted on the map. The areas in the slabs where undulations corresponding to these scales are present are shown.

#### 4.3.2 Surface analysis and automatic defect detection

Figure 8 illustrates regions, enclosed by ellipses, where potential defects have been identified for two of the five scales in Figure 7. Note that no defective regions were found for the other three scales.

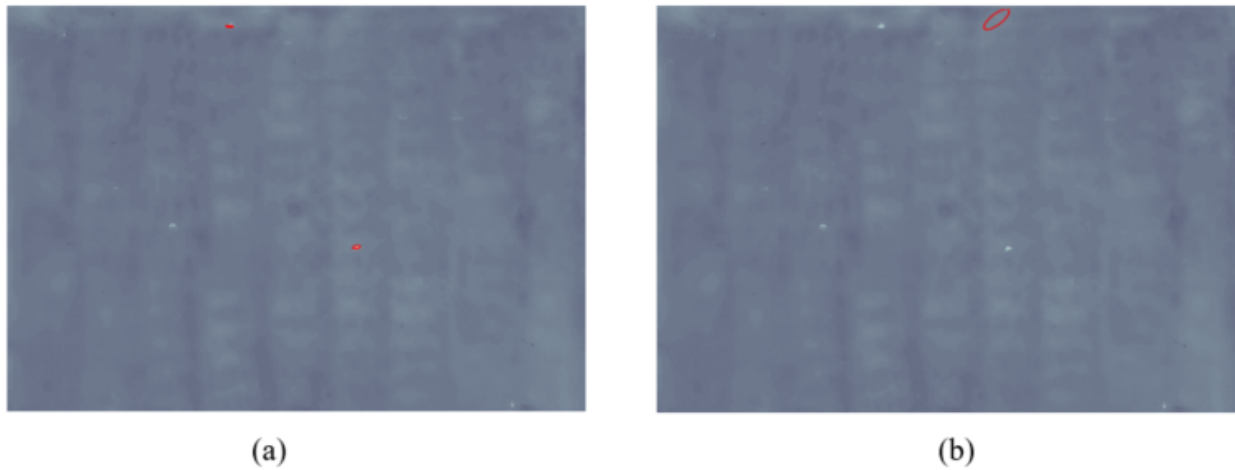


Figure 8 Potential defective areas for a) 61cm ( $\pm 2$ cm) and b) 244cm ( $\pm 2$ cm).

The advantage of our approach is that it combines dense 3D data from TLS with the 2D CWT that can support the analysis of waviness with essentially any characteristic period (i.e. wavelength). This enables our approach to study waviness not just for a few discrete wavelengths (like the 5 above), but for dense and large ranges of wavelengths. This is demonstrated in Figure 9 that summarizes the potential defects on the slab for any wavelength within the continuous range of 20 to 400 cm.



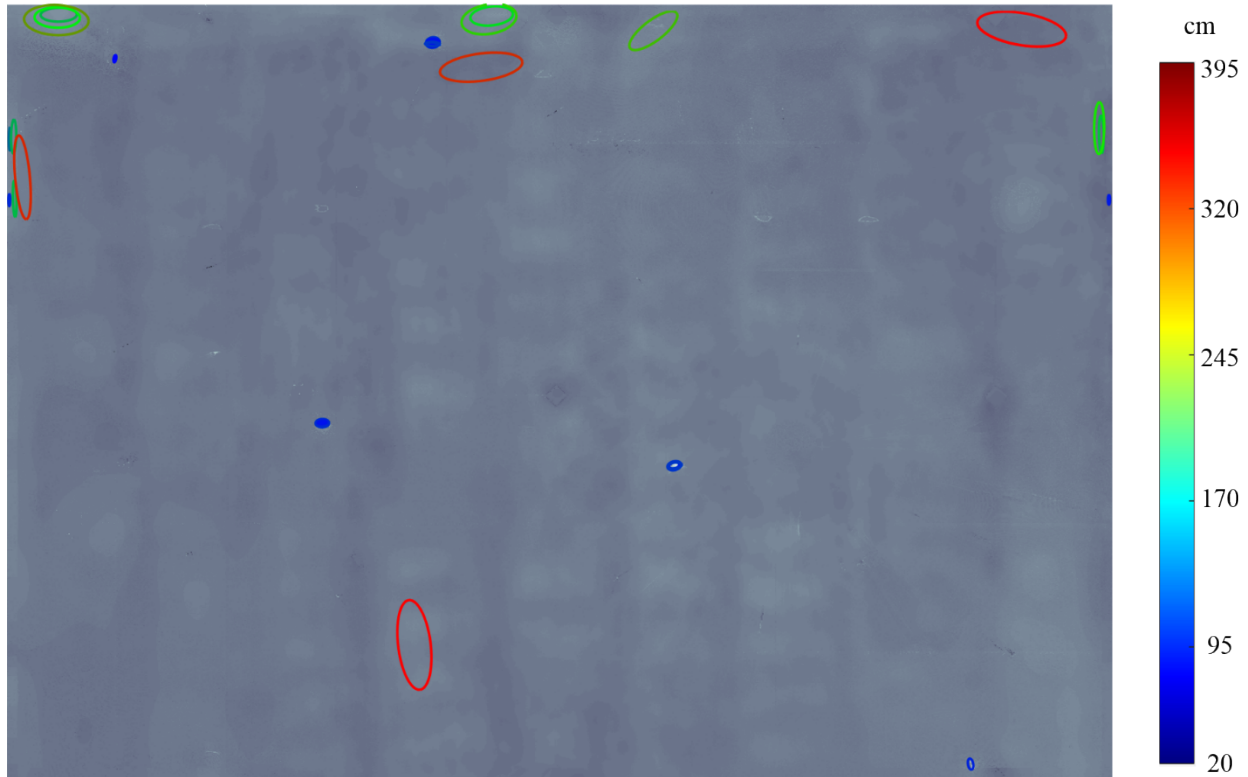


Figure 9 Detected defects for periods between 20 and 400 cm.

#### 4.4 Comparison of Results with WI method

The ASTM E1486-14 standard describes the test method for measuring the waviness of concrete floors using the WI method. In a similar way to [8], we propose to apply the WI method as defined in this standard, but using the digitized slab surface as the surface of application (instead of the real slab). Referring to this standard, 103 survey lines along the x-axis and 148 lines along the y-axis were defined on the slab, as shown in Figure 10. The lines are spaced at 1-ft intervals. This is much denser than what would normally be achieved in normal practice, but is useful to conduct the comparison with the proposed CWT approach.

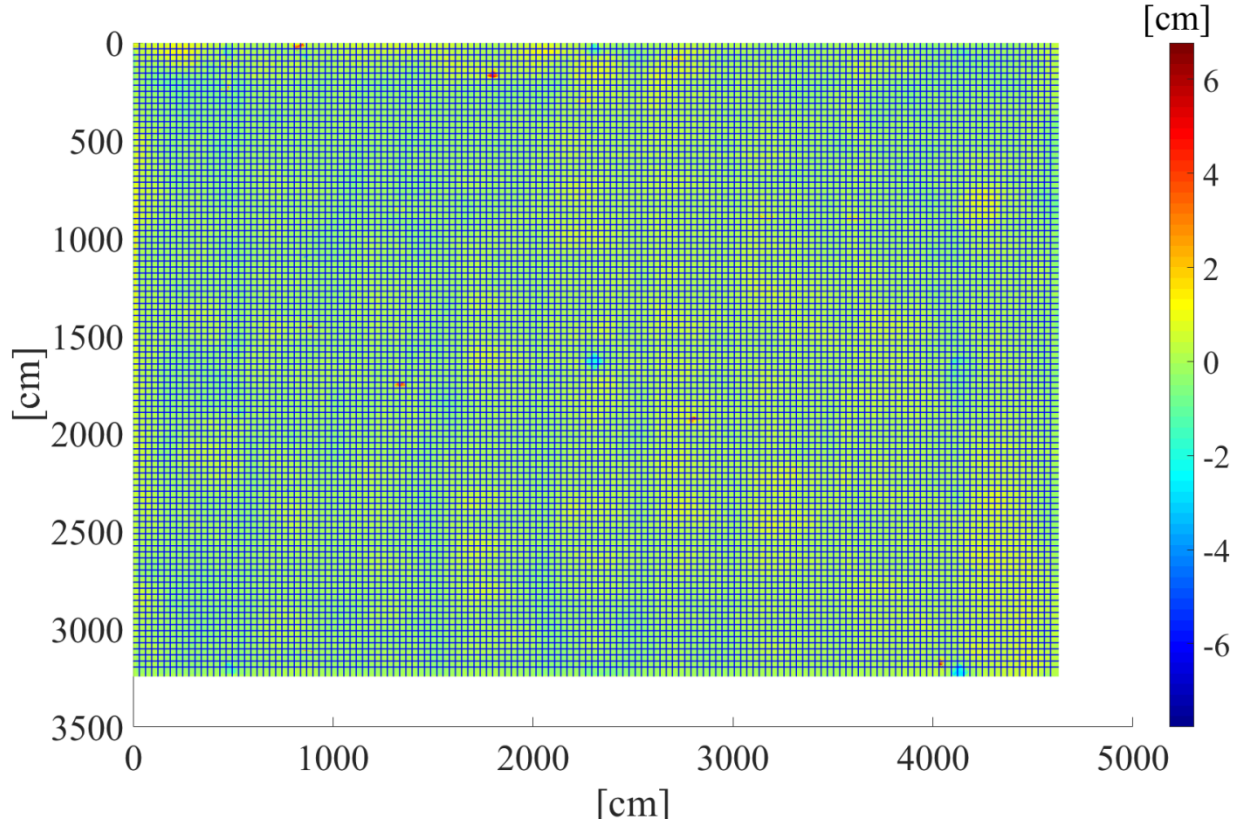


Figure 10 The 251 survey lines (103 along the x-axis and 148 along the y-axis) that are defined across the slab surface.

The length adjusted RMS deviation ( $LAD$ ) responses are calculated for each line. The survey lines are parallel to each other and are spaced at a distance of 30.5 cm (1 ft). Survey points with a spacing  $s=30.5$  cm (1 ft) are measured along those lines. The standard defines chord length as the length of the imaginary line joining two points on the surface of the concrete floor. The chord length is equal to  $2ks$ , where  $k= \{1, 2, 3, 4 \text{ and } 5\}$ . The vertical distance between the midpoint of the chord and the survey point on the surface,  $D_{kj}$ , is calculated using the following formula,

$$D_{kj} = h_{j+k} - 0.5(h_j + h_{j+2k}) \quad (6)$$

where,  $h_{j+k}$ ,  $h_j$  and  $h_{j+2k}$  represent the heights of the survey point and the two end points of the chord, respectively. These heights are obtained from the depth map calculated in section 4.2.

After the deviation  $D_{kj}$  is calculated, the length adjusted RMS deviation ( $LAD_k$ ) is calculated using equation 7.

$$LAD_{l,k} = \sqrt{\frac{L_r}{2ks} [\sum_{i=1}^{jmax_{l,k}} (D_{l,k,j})^2]} \quad (7)$$

where  $L_r$  corresponds to the reference length of 1 ft.  $jmax_k$  corresponds to the total number of deviation calculations with a chord length  $2ks$  along a survey line and  $l$  denotes the survey line being tested.

Similarly, the 2D CWT responses at the  $j^{\text{th}}$  sampled location,  $CWT_{l,a,j}$ , for scales 15, 30, 45, 60 and 75 were obtained in section 4.3.1. These scales correspond to the WI k-values 1, 2, 3, 4 and 5 respectively. It is proposed that the CWT responses for each of the 210 lines for those 5 scales,  $CWT_{l,a}$ , be calculated using the similar formula:

$$CWT_{l,a} = \sqrt{\frac{\sum_{i=1}^{jmax_{l,a}} CWT_{l,a,j}^2}{jmax_{l,a}}} \quad (8)$$

where  $jmax_k$  corresponds to number of locations at which the 2D CWT response have been calculated.

The correlation between the  $LAD_{l,k}$  and  $CWT_{l,a}$  responses is calculated to compare the surface waviness results obtained using the WI and 2D CWT methods. 15 survey lines along the x-axis and 15 survey lines along the y-axis, as shown in Figure 11, are randomly selected (out of the previously defined 251 lines), to illustrate the correlation results presented in Figure 12 and Figure 13. The correlation coefficients, denoted by  $r^2$ , are included in the top left-hand corner of each graph. The values indicate a strong correlation between the results obtained using the WI and 2D CWT methods. This strongly validates the value of the proposed approach, which has the additional advantage of being able to more precisely define defects' wavelengths and locations (including actual orientation).



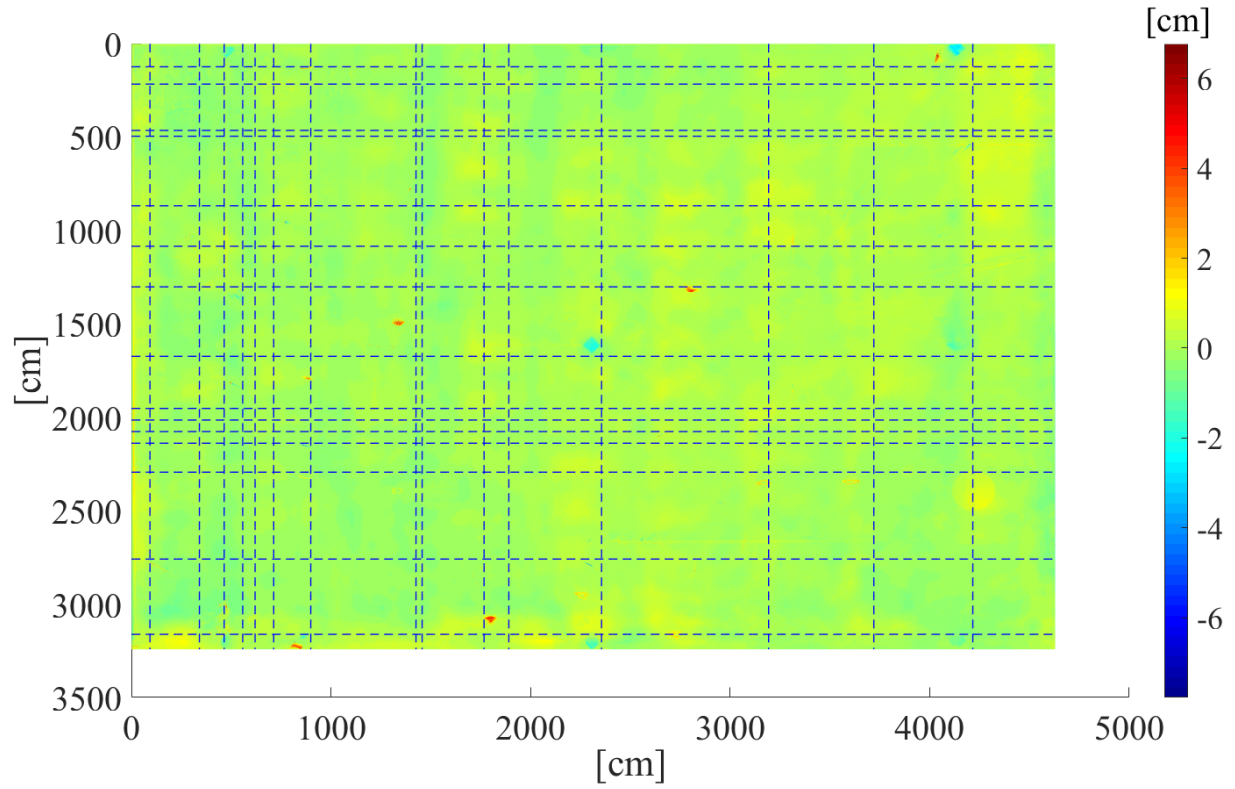


Figure 11 The 30 survey lines (15 along each axis) that were selected for the generation of correlation results.

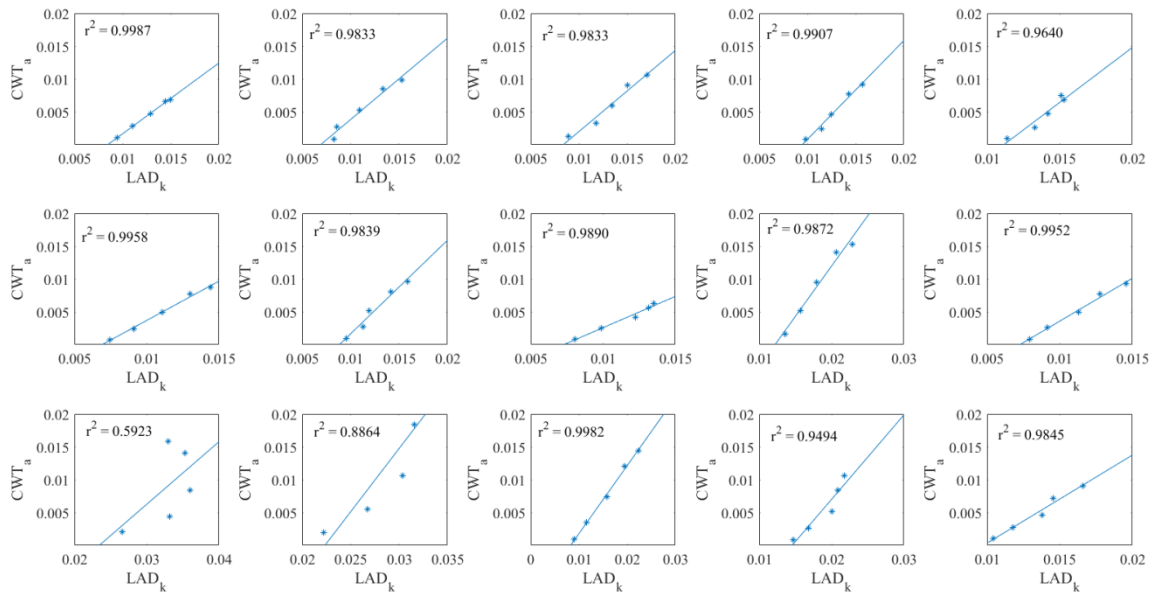


Figure 12 Correlation between  $LAD_{l,k}$  and  $CWT_{l,a}$  responses for the five characteristic undulation periods [61, 121.9, 182.9, 243.8, 304.8] cm, along 16 lines along the x-axis shown in Figure 11.

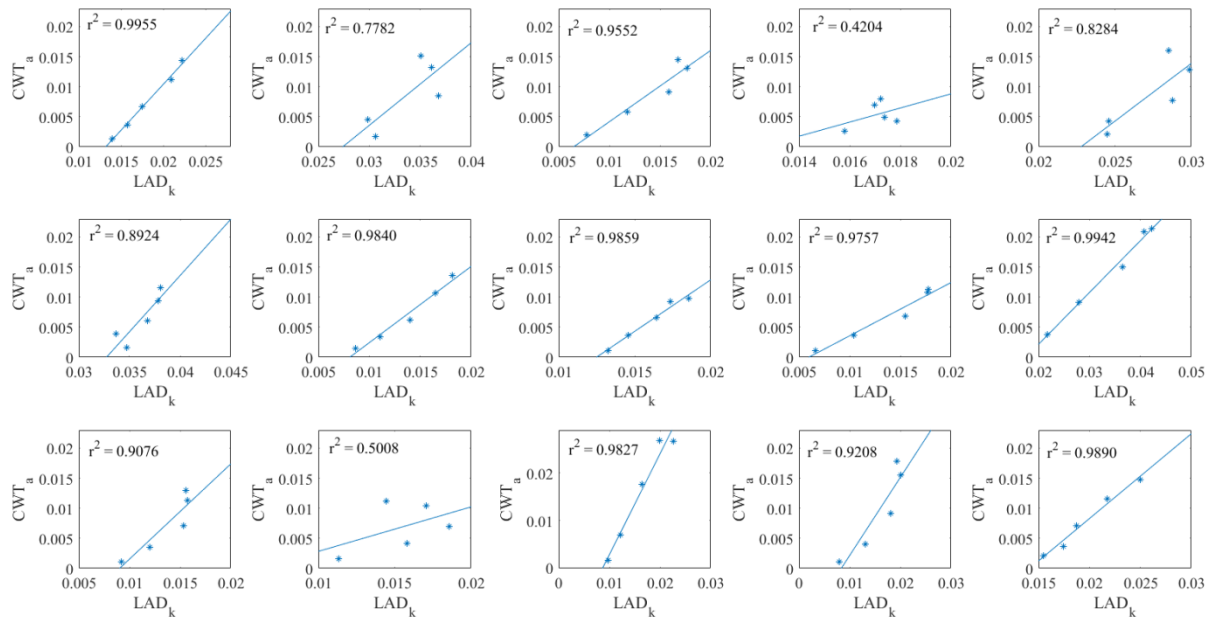


Figure 13 Correlation between  $LAD_{l,k}$  and  $CWT_{l,a}$  responses for the five characteristic undulation periods [61, 121.9, 182.9, 243.8, 304.8] cm, along 16 lines along the y-axis shown in Figure 11.

The proposed approach overcomes all of the drawbacks of traditional waviness assessment methods mentioned earlier. The 2D CWT method enables a comprehensive analysis of the waviness of 2D surfaces, both in the spatial and wavelength domains. In contrast to the F-number and WI methods, the output of the CWT-based approach enables easy visual representations of where waviness defects are located on the surface (as shown in Figure 7). This can help users with minimal knowledge about 3D TLS or 2D CWT to quickly determine where surface corrections should be applied, for example.

## 5 Conclusions

TLS technology has a promising future in the construction industry owing to its ability to rapidly and accurately capture and record as-built conditions. Research efforts are being concentrated to identify specific areas, which could particularly benefit from the application of TLS. Dimensional QC is one such area. The analysis performed using the 2D CWT for QC provides great flexibility for examining the surface undulations with a wide range of characteristic

periods. The localization property of 2D CWT highlights regions on the surface and helps in compliance assessment and corrective work planning.

The proposed approach in this paper demonstrates how TLS data of a concrete surface can be used to characterize waviness by implementing 2D CWT, using Mexican Hat Wavelet as the mother wavelet. The comparative analysis of the various methods of measuring waviness in concrete slabs reveals that the 2D CWT method provides results that strongly correlate with those of the WI method (the current state of the art), but has numerous advantages over it and other existing methods.

Future research efforts can be directed toward improving the practicality of implementing laser scanning for measuring floor surface waviness. The method proposed in this paper can be used in conjunction with augmented reality devices to enable the visualization of undulations corresponding to various characteristic periods on site. The proposed method can be further improved by developing algorithms for automatically removing noise and generating scan plans to estimate optimal scanning positions. For this study, manual effort was required for preparing scan plans, setting up the scanner and collecting the point cloud data. A LiDAR integrated Unmanned Aerial Vehicle (UAV) can also be used to collect the scans and automated registration of laser scans can be further explored. Finally, a comparative analysis on using TLS and LiDAR equipped UAVs for surface quality assessment can be conducted.

## Acknowledgement

The authors would like to thank Chris McInroe, Jeff Perala and Laine Perala from Perlo Construction for allowing the collection of laser scan data from the Vista Logistics Park project in Gresham, OR.

## References

- [1] D.K. Ballast, Handbook of construction tolerances, John Wiley, Hoboken, 2007, ISBN: 978-0-471-93151-5
- [2] Manual for quality control for plants and production of structural precast concrete products, Precast/Prestressed Concrete Institute, Chicago, IL, 1999, [http://www.enconunited.com/wp-content/uploads/2017/07/pci\\_mnl-116-99\\_structural\\_qc\\_manual.pdf](http://www.enconunited.com/wp-content/uploads/2017/07/pci_mnl-116-99_structural_qc_manual.pdf)

- [3] H.P. Gillette, C.S. Hill, C.T. Murray, H.B. Kirkland, S.C. Hadden, Engineering and Contracting, The Myron C. Clark Publishing Company, 1913.
- [4] J. L. Burati, J. J. Farrington, Costs of quality deviations in design and construction. Bureau of Engineering Research, University of Texas at Austin, 1987.
- [5] L. Patterson, W.B. Ledbetter, The Cost of Quality: A Management Tool, Excellence in the Construction Project, American Society of Civil Engineers, 1989, pp. 100-105.
- [6] P.-E. Josephson, Y. Hammarlund, The causes and costs of defects in construction, Automation in Construction. 8 (1999) 681–687, [https://doi.org/10.1016/s0926-5805\(98\)00114-9](https://doi.org/10.1016/s0926-5805(98)00114-9)
- [7] P. Tang, B. Akinci, D. Huber, Characterization of three algorithms for detecting surface flatness defects from dense point clouds, Three-Dimensional Imaging Metrology. (2009), <https://doi.org/10.1117/12.805727>.
- [8] F. Bosché, B. Biotteau, Terrestrial laser scanning and continuous wavelet transform for controlling surface flatness in construction – A first investigation, Advanced Engineering Informatics. 29 (2015) 591–601, <https://doi.org/10.1016/j.aei.2015.05.002>.
- [9] F.R. Neal, Concrete industrial ground floors, Thomas Telford, London, 2002.
- [10] B.M. Phares, G.A. Washer, D.D. Rolander, B.A. Graybeal, M. Moore, Routine Highway Bridge Inspection Condition Documentation Accuracy and Reliability, Journal of Bridge Engineering. 9 (2004) 403–413, [https://doi.org/10.1061/\(asce\)1084-0702\(2004\)9:4\(403\)](https://doi.org/10.1061/(asce)1084-0702(2004)9:4(403)).
- [11] ASTM E1155-14 Standard Test Method for Determining FF Floor Flatness and FL Floor Levelness Numbers, ASTM International, West Conshohocken, PA, 2014, <https://doi.org/10.1520/E1155-14>
- [12] ASTM E1486-14 Standard Test Method for Determining Floor Tolerances Using Waviness, Wheel Path and Levelness Criteria, ASTM International, West Conshohocken, PA, 2014, <https://doi.org/10.1520/E1486>
- [13] C. N. Ytterberg, Using the Waviness Index To Improve Floor Flatness (1996). [http://www.concreteconstruction.net/\\_view-object?id=00000153-8bb9-dbf3-a177-9fb958f40000](http://www.concreteconstruction.net/_view-object?id=00000153-8bb9-dbf3-a177-9fb958f40000)
- [14] R. E. Loov, Is the F-number system valid for your floor?, Concrete International. 12 (1990) 68–76. <https://www.concrete.org/publications/internationalconcreteabstractsportal/m/details/id/3252>
- [15] DIN 18202 Tolerances in building construction – Buildings, Deutsches Institut für Normung e. V., 2005.
- [16] Latta, J. K., Inaccuracies in construction, Cracks, movements and joints in buildings, National research council of Canada. (1976) 171.

- [17] G.S. Cheok, W.C. Stone, R.R. Lipman, C. Witzgall, Ladars for construction assessment and update, *Automation in Construction*. 9 (2000) 463–477, [https://doi.org/10.1016/s0926-5805\(00\)00058-3](https://doi.org/10.1016/s0926-5805(00)00058-3).
- [18] H. Son, C. Kim, Semantic as-built 3D modeling of structural elements of buildings based on local concavity and convexity, *Advanced Engineering Informatics*. 34 (2017) 114–124, <https://doi.org/10.1016/j.aei.2017.10.001>.
- [19] S. Tuttas, A. Braun, A. Borrmann, U. Stilla, Comparision of photogrammetric point clouds with BIM building elements for construction progress monitoring, *ISPRS - International Archives of the Photogrammetry, Remote Sensing and Spatial Information Sciences*. XL-3 (2014) 341–345, <https://doi.org/10.5194/isprsarchives-xl-3-341-2014>.
- [20] A. Braun, S. Tuttas, A. Borrmann, U. Stilla, A concept for automated construction progress monitoring using BIM-based geometric constraints and photogrammetric point clouds, *Journal of Information Technology in Construction (ITcon)* 20 (5) (2015) 68-79, <http://www.itcon.org/2015/5>
- [21] A. Braun, S. Tuttas, A. Borrmann, U. Stilla, Automated Progress Monitoring Based on Photogrammetric Point Clouds and Precedence Relationship Graphs, *Proceedings of the 32nd International Symposium on Automation and Robotics in Construction and Mining (ISARC 2015)*. (2015), <https://doi.org/10.22260/isarc2015/0034>.
- [22] C. Kim, H. Son, C. Kim, Automated construction progress measurement using a 4D building information model and 3D data, *Automation in Construction*. 31 (2013) 75–82, <https://doi.org/10.1016/j.autcon.2012.11.041>.
- [23] H. Son, C. Kim, Y.K. Cho, Automated Schedule Updates Using As-Built Data and a 4D Building Information Model, *Journal of Management in Engineering*. 33 (2017) 04017012, [https://doi.org/10.1061/\(asce\)me.1943-5479.0000528](https://doi.org/10.1061/(asce)me.1943-5479.0000528).
- [24] M.-C. Amann, T. Bosch, M. Lescure, R. Myllyla, M. Rioux, “Laser ranging: a critical review of unusual techniques for distance measurement, *Optical Engineering*. 40 (1) (2001) 10-20, <https://doi.org/10.1117/1.1330700>
- [25] P. A. Fuchs, G. A. Washer, S. B. Chase, M. Moore, Applications of Laser-Based Instrumentation for Highway Bridges, *Journal of Bridge Engineering* 9 (6) (2004) 541-549, [https://doi.org/10.1061/\(ASCE\)1084-0702\(2004\)9:6\(541\)](https://doi.org/10.1061/(ASCE)1084-0702(2004)9:6(541))
- [26] T. Schafer, T. Weber, Deformation measurement using terrestrial laser scanning at the hydropower station of Gabcikovo, *INGEO 2004 and FIG Regional Central and Eastern European Conference on Engineering Surveying, FIG, Copenhagen, Denmark.*, 2004.
- [27] M.C. Israel, R.G. Pileggi, Use of 3D laser scanning for flatness and volumetric analysis of mortar in facades, *Revista IBRACON De Estruturas e Materiais*. 9 (2016) 91–122, <https://doi.org/10.1590/s1983-41952016000100007>.

- 544 [28] Q. Wang, M.K. Kim, J.C. Cheng, H. Sohn, Automated quality assessment of precast  
545 concrete elements with geometry irregularities using terrestrial laser scanning, *Automation*  
546 *in Construction*. 68 (2016) 170–182, <https://doi.org/10.1016/j.autcon.2016.03.014>.
- 547 [29] N.J. Shih, P.H. Wang, Using point cloud to inspect the construction quality of wall finish,  
548 *Proceedings of the 22nd eCAADe Conference*, 2004, pp. 573–578,  
549 [http://papers.cumincad.org/data/works/att/2004\\_573.content.pdf](http://papers.cumincad.org/data/works/att/2004_573.content.pdf)
- 550 [30] F. Bosché, E. Guenet, Automating surface flatness control using terrestrial laser scanning  
551 and building information models, *Automation in Construction*. 44 (2014) 212–226.  
552 <https://doi.org/10.1016/j.autcon.2014.03.028>.
- 553 [31] E. Valero, F. Bosché, Automatic Surface Flatness Control using Terrestrial Laser Scanning  
554 Data and the 2D Continuous Wavelet Transform, *Proceedings of the 33rd International*  
555 *Symposium on Automation and Robotics in Construction (ISARC)*. (2016),  
556 <https://doi.org/10.22260/isarc2016/0007>.
- 557 [32] P. Goupillaud, A. Grossmann, J. Morlet, Cycle-octave and related transforms in seismic  
558 signal analysis, *Geoexploration*. 23 (1984) 85–102, [https://doi.org/10.1016/0016-](https://doi.org/10.1016/0016-7142(84)90025-5)  
559 [7142\(84\)90025-5](https://doi.org/10.1016/0016-7142(84)90025-5).
- 560 [33] R. Kronland-Martinet, J. Morlet, A. Grossmann, Analysis Of Sound Patterns Through  
561 Wavelet Transforms, *International Journal of Pattern Recognition and Artificial*  
562 *Intelligence*. 01 (1987) 273–302, <https://doi.org/10.1142/s0218001487000205>.
- 563 [34] T. Paul, Functions analytic on the half-plane as quantum mechanical states, *Journal of*  
564 *Mathematical Physics*. 25 (1984) 3252–3263, <https://doi.org/10.1063/1.526072>.
- 565 [35] J. Raja, B. Muralikrishnan, S. Fu, Recent advances in separation of roughness, waviness  
566 and form, *Precision Engineering*. 26 (2002) 222–235, [https://doi.org/10.1016/s0141-](https://doi.org/10.1016/s0141-6359(02)00103-4)  
567 [6359\(02\)00103-4](https://doi.org/10.1016/s0141-6359(02)00103-4).
- 568 [36] Y. Ge, H. Tang, M.A.M.E. Eldin, P. Chen, L. Wang, J. Wang, A Description for Rock Joint  
569 Roughness Based on Terrestrial Laser Scanner and Image Analysis, *Scientific Reports*. 5  
570 (2015), <https://doi.org/10.1038/srep16999>.
- 571 [37] M. Bitenc, D.S. Kieffer, K. Khoshelham, Evaluation Of Wavelet Denoising Methods For  
572 Small-Scale Joint Roughness Estimation Using Terrestrial Laser Scanning, *ISPRS Annals*  
573 *of Photogrammetry, Remote Sensing and Spatial Information Sciences*. II-3/W5 (2015) 81–  
574 88, <https://doi.org/10.5194/isprsannals-ii-3-w5-81-2015>.
- 575 [38] K. Khoshelham, D. Altundag, Wavelet De-Noising of Terrestrial Laser Scanner Data for  
576 the Characterization of Rock Surface Roughness, *The International Archives of the*  
577 *Photogrammetry, Remote Sensing and Spatial Information Sciences*. 38 (1998) 373–378.  
578 [https://repository.tudelft.nl/islandora/object/uuid%3A520bf4ee-388c-4848-a8ec-](https://repository.tudelft.nl/islandora/object/uuid%3A520bf4ee-388c-4848-a8ec-70eabcfafc50)  
579 [70eabcfafc50](https://repository.tudelft.nl/islandora/object/uuid%3A520bf4ee-388c-4848-a8ec-70eabcfafc50)

- [39] X. Chen, J. Raja, S. Simanapalli, Multi-Scale Analysis of Engineering Surfaces, *International Journal of Machine Tools and Manufacture*. 35 (2) (1995) 231–238, [https://doi.org/10.1016/0890-6955\(94\)P2377-R](https://doi.org/10.1016/0890-6955(94)P2377-R)
- [40] B. Josso, D.R. Burton, M.J. Lalor, Frequency normalised wavelet transform for surface roughness analysis and characterisation, *Wear*. 252 (2002) 491–500, [http://dx.doi.org/10.1016/s0043-1648\(02\)00006-6](http://dx.doi.org/10.1016/s0043-1648(02)00006-6).
- [41] K. Stępień, W. Makiela, An Analysis of Deviations of Cylindrical Surfaces with the Use of Wavelet Transform, *Metrology and Measurement Systems*. 20 (2013), <http://dx.doi.org/10.2478/mms-2013-0013>.
- [42] X. Jiang, L. Blunt, K. Stout, Lifting wavelet for three-dimensional surface analysis, *International Journal of Machine Tools and Manufacture*. 41 (2001) 2163–2169, [http://dx.doi.org/10.1016/s0890-6955\(01\)00083-9](http://dx.doi.org/10.1016/s0890-6955(01)00083-9).
- [43] R. R. Coifman, M. Maggioni, Diffusion Wavelets, *Applied and Computational Harmonic Analysis*. 21 (1) (2006) 53–94. doi: <https://doi.org/10.1016/j.acha.2006.04.004>
- [44] H.S. Abdul-Rahman, X.J. Jiang, P.J. Scott, Freeform surface filtering using the lifting wavelet transform, *Precision Engineering*. 37 (2013) 187–202, <http://dx.doi.org/10.1016/j.precisioneng.2012.08.002>.
- [45] D. Mendlovic, N. Konforti, Optical realization of the wavelet transform for two-dimensional objects, *Applied Optics*. 32 (1993) 6542, <http://dx.doi.org/10.1364/ao.32.006542>.
- [46] V.V. Valenzuela, R.D. Lins, H.M.D. Oliveira, Application of Enhanced-2D-CWT in Topographic Images for Mapping Landslide Risk Areas, *Lecture Notes in Computer Science Image Analysis and Recognition*. (2013) 380–388, [http://dx.doi.org/10.1007/978-3-642-39094-4\\_43](http://dx.doi.org/10.1007/978-3-642-39094-4_43).
- [47] R. Polikar, *The Wavelet Tutorial. The Engineer's Ultimate Guide to Wavelet Analysis*, 2006.
- [48] P.S. Addison, *The illustrated wavelet transform handbook: introductory theory and applications in science, engineering medicine and finance*, CRC Press, Boca Raton, 2017, ISBN: 9781482251326
- [49] I. Daubechies, *Ten lectures on wavelets*, Society for Industrial and Applied Mathematics, Philadelphia, PA, 1992, <https://doi.org/10.1137/1.9781611970104>
- [50] N. Wang, C. Lu, Two-Dimensional Continuous Wavelet Analysis and Its Application to Meteorological Data, *Journal of Atmospheric and Oceanic Technology*. 27 (2010) 652–666, <http://dx.doi.org/10.1175/2009jtecha1338.1>.
- [51] J.-P. Antione, R. Murenzi, P. Vandergheynst, S. T. Ali, *Two-dimensional wavelets and their relatives*, Cambridge University Press, Cambridge, 2008, <https://doi.org/10.1017/CBO9780511543395>



- 617 [52] R. Leach, Characterisation of Areal Surface Texture, Springer Berlin, Berlin, 2013,  
618 <https://doi.org/10.1007/978-3-642-36458-7>
- 619 [53] R.X. Gao, R. Yan, Wavelets - Theory and applications for manufacturing, Springer, New  
620 York, 2011, <https://doi.org/10.1007/978-1-4419-1545-0>
- 621 [54] W.X. Yang, X.M. Ren, Detecting impulses in mechanical signals by wavelets, EURASIP  
622 Journal on Applied Signal Processing. 2004 (2004) 1156-1162,  
623 <https://doi.org/10.1155/S1110865704311091>
- 624 [55] D. Marr, E. Hildreth, Theory of Edge Detection, Proceedings of the Royal Society London.  
625 Series B, Biological Sciences. 207 (1167) (1980) 187-217,  
626 <http://dx.doi.org/10.1098/rspb.1980.0020>.
- 627 [56] J. P. Antoine, R. Murenzi, Two-dimensional directional wavelets and the scale-angle  
628 representation, Signal Processing, 52 (3) (1996) 259-281, [https://doi.org/10.1016/0165-](https://doi.org/10.1016/0165-1684(96)00065-5)  
629 [1684\(96\)00065-5](https://doi.org/10.1016/0165-1684(96)00065-5).
- 630 [57] ACI Committee 117, ACI 117-10 Specification for Tolerances for Concrete Construction  
631 and Materials and Commentary. 2010, ISBN: [9780870313790](https://doi.org/10.1007/9780870313790)
- 632 [58] S. Kunis, Nonequispaced FFT: generalisation and inversion, Shaker, Aachen, 2007, ISBN  
633 [3832258787](https://doi.org/10.1007/978332258787)
- 634 [59] Leica Geosystems, Leica ScanStation P30/P40 product specifications, 2016. [http://w3.leica-](http://w3.leica-geosystems.com/downloads123/hds/hds/general/brochures-datasheet/Leica_ScanStation_P30-P40_Plant_DS_en.pdf)  
635 [geosystems.com/downloads123/hds/hds/general/brochures-](http://w3.leica-geosystems.com/downloads123/hds/hds/general/brochures-datasheet/Leica_ScanStation_P30-P40_Plant_DS_en.pdf)  
636 [datasheet/Leica\\_ScanStation\\_P30-P40\\_Plant\\_DS\\_en.pdf](http://w3.leica-geosystems.com/downloads123/hds/hds/general/brochures-datasheet/Leica_ScanStation_P30-P40_Plant_DS_en.pdf)
- 637